Effect of Air Channel Depth and Mass Flow Rate on the Efficiency of Hybrid Thermal - Photovoltaic Sensor

M Lyes*, K Tahar, H Ouided, C Hamid
Physics Department, Exact Sciences Faculty, Physics Chemistry of Semi-Conductor Laboratory, Constantine University, Constantine

ABSTRACT
We present in this paper the effect of the mass flow rate and air channel depth on the efficiency of hybrid thermal-photovoltaic sensor. A numerical simulation of the performance of the thermal-photovoltaic sensor with a heat exchanger including fins attached to the absorber and using air as a coolant is presented. A thorough analysis of the mass flow rate, and air channel depth influence on the efficiency and the working of the system are examined. We use the heat transfer equations cascade of the components as a matrix of four unknown's temperatures, which are the glass, cells, fluid and insulation plate temperatures. To solve this matrix, the fixed point and Gauss-Seidel method, at the transitory regime are used. Results at solar irradiance of 1120 W/m2 show that the combined thermal-photovoltaic efficiency is increasing from 60% to 75% and the mass flow rate necessary to maintain the cells at a constant temperature is decreasing form 1.8 to 1.2 Kg/s, when the exchanger channel depth varies from 0.35 to 0.05 m. The overall conversion efficiency of the system increases from 25% to 60%, and the cell temperature decreases from 345K to 335K when mass flow rate changes from 0.02 kg/s to 0.1 kg/s.

1. INTRODUCTION

The environmental pollution and the energy lack become a much serious problem. Renewable and environment friendly, solar energy is the solution to the energy global demand in the future. The Methods for the conversion of solar energy can be classified into two types: photo thermal solar energy is converted into heat and subsequently transformed into electricity. The photovoltaic methods converted solar energy into electricity directly. Usually, these two methods separately give a low efficiency of convection. The combination of photovoltaic and photo thermal components, leads to a hybrid system which improve the conversion efficiency because it produces both electricity and heat. When the sunlight is concentrated on the solar cell, the absorbed energy increases the cell temperature and reduces the electrical efficiency. Therefore, it is necessary to remove the heat from the cell by a heat transfer fluid (air, water…). To reduce the temperature of solar cell, kern and all presented a prototype of a thermal-photovoltaic system with air and water as coolant fluids in 1978 [1]. A great number of theoretical and experimental studies to assess the efficiency of hybrid thermal-photovoltaic system have been performed. To provide domestic hot water Flor schuetz and all analyze the

*Corresponding Author: maifi@umc.edu.dz

performance of the hybrid solar system with the hotel-Whillier model [2]. Garg and all have developed a stable model to simulate the performance of thermal-photovoltaic hybrid system [3]. In the recent years much research has been reported in the literature on new solar thermal systems with lower costs [4-7]. In this work we analyze the mass flow rate and the exchanger channel depth effects on the efficiency of the system when the length of the system, the cell parameters (V, I, T…..) and the cooling by the exchanger vary.

2. SYSTEM MODEL

The system model as seen in the figure 1 consists of two parts:

In one part, we calculate the thermal parameters of the system, as temperature (T), and thermal efficiency of the sensor (Effth). The second part is devoted to the electrical model; in which we calculate the electrical intensity (I), the voltage (V) and the generated electric power. The hybrid thermal-photovoltaic collector considered in this work is shown in figure1. The plastic glass cover is inserted to protect the sensor against mechanical damage. The light is reflected and concentrated on the solar cell by two reflexive cylindro-parabolic concentrators. The focusing system consists of the cylindro-parabolic concentrators. Each one focuses the light on a panel with 36 cells connected in series (Generic 60 Wp polycrystalline).The two panels are also connected in series along the direction of the system. They are glued and sealed to keep cells surface clean. Fins are fixed on the heat exchanger to improve heat transfer from the solar cells to the fluid. The heat exchanger bottom is covered with a good insulator to minimize heat losses to the ambient [7].The cold air enters the exchanger through a centrifugal compressor; the latter is powered by an alternating current. The controller convert a power generating part continues by alternative power cells so that the compressor works. The compound parabolic concentrator is a non-imaging line-axis concentrator, which consists of two reflectors concentrating the radiation from aperture to absorber. All rays incident on the aperture inside the acceptance angle as shown in figure 1. It is a designed based on the edge-ray principle. Because the mirror area of high concentrating ration is too large, it is necessary to cut off the top portion of reflectors, and this does not loss much radiation in concentrator. In this paper, the concentrating ratio is selected as 2, the reflectors is truncated by third height. The detail optical and thermal of the compound parabolic concentrator is adopted from reference [11].

3. THERMAL MODEL

Figure 2 shows the thermal model of the system. For the sake of simplicity, the following assumptions are made in permanent regime:

- The heat transfer process is one dimensional and in a steady state.
- The heat capacities of the glass cover, concentrator, solar cell, fins, absorber and insulating plate are negligible.
- The parabolic concentrator is ideal and all incident radiations with in acceptance angle can reach the solar cells.
- The solar radiations converted into thermal energy are completely absorbed by the panels and solar absorber.
- The temperature of the solar cell and absorber are uniform.

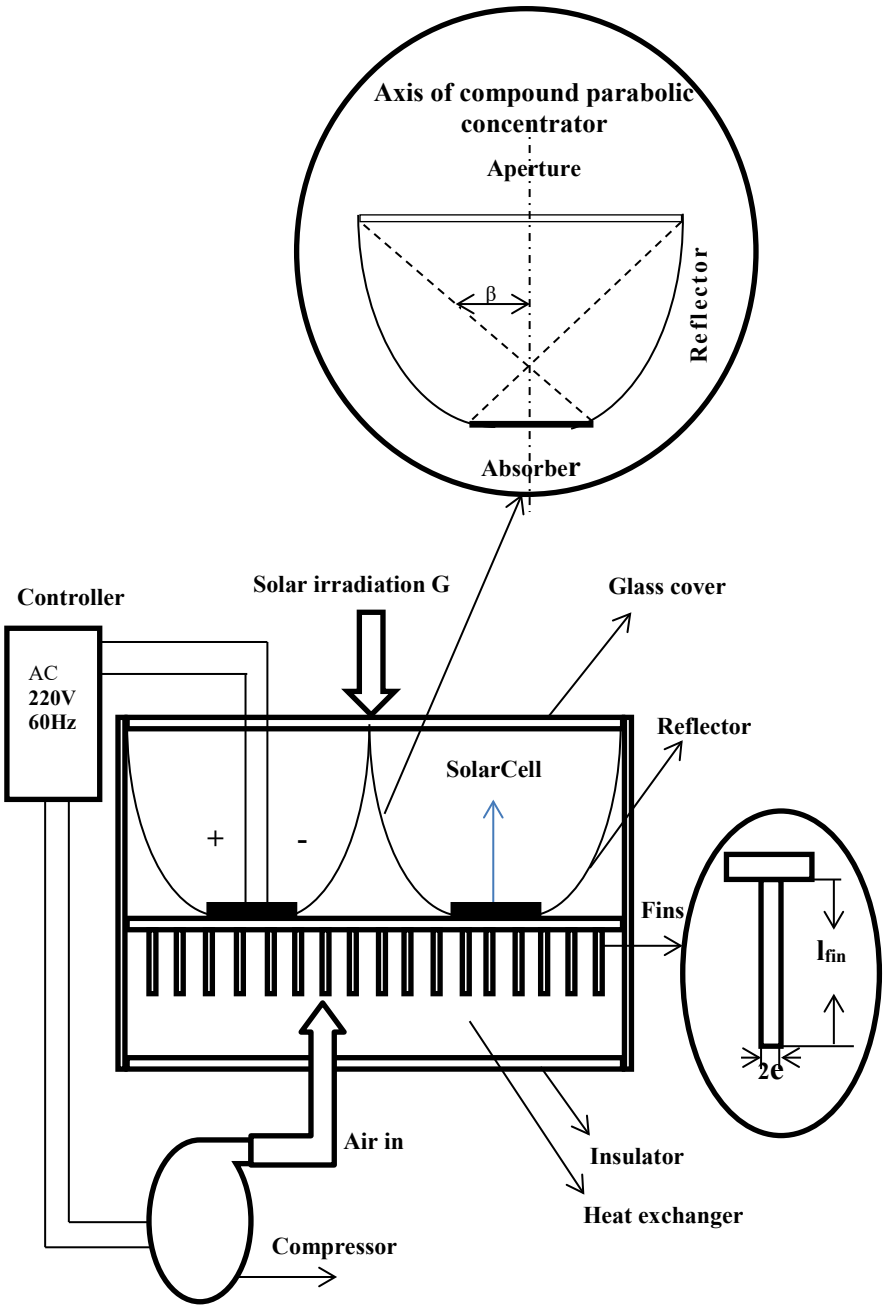

Figure 1. Schematic view of our sensor photovoltaic-thermal

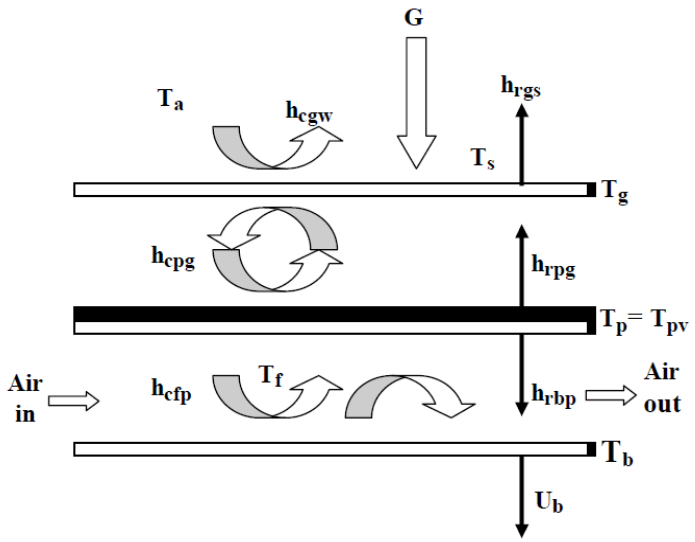

Figure 2. Thermal model of our thermal-photovoltaic sensor

Based on the above assumptions, the energy equations can be written as

3.1. For the glass cover

We have

$$m_g C_g \frac{\partial T_g}{\partial t} + \alpha_g G Co\left(1 + \tau_g \rho_g \rho_R^{2n}\right) = h_{rgs}\left(T_g - T_s\right) + h_{cgw}\left(T_g - T_w\right) + h_{cpg}\left(T_g - T_p\right) + \frac{A_{ct}}{A} h_{rpg}\left(T_g - T_p\right) \quad (1)$$

Where n is the average number of reflection for radiation inside the acceptance angle, and Co is the ratio concentrating.

3.2. At the photovoltaic thermal plate

We have

$$m_p C_p \frac{\partial T_p}{\partial t} + \tau_g \alpha_p G \rho_R^n d\left(1 + \frac{\rho_p \rho_g \rho_R^{2n}}{Co}\right)(1 - F) + \tau_g \alpha_p G F \rho_R^n d\left(1 + \frac{\rho_{pv} \rho_g \rho_R^{2n}}{Co}\right)\left(1 - Eff_{pv}\right) = \frac{A_{cb}}{A} h_{cpf}\left(T_p - T_f\right) Eff_p + \frac{A_{cb}}{A} h_{rpb}\left(T_p - T_b\right) + \frac{A_{ct}}{A} h_{cpg}\left(T_P - T_g\right) + \frac{A_{ct}}{A} h_{rpg}\left(T_p - T_g\right) \quad (2)$$

Where d is the correction of gap loss. F is the solar cell packing factor with [8-11].

Eff_p: is the plate efficiency

$$Eff_p = \frac{A + A_{fin} Eff_{fin}}{A_{cb}}$$

$$\mathrm{Eff_{fin}} = \frac{\tanh\left(\mathrm{l_{fin}}\sqrt{\left(\frac{\mathrm{h_{cpf}}}{\mathrm{e}\lambda_{\mathrm{fin}}}\right)}\right)}{\mathrm{l_{fin}}\sqrt{\left(\frac{\mathrm{h_{cpf}}}{\mathrm{e}\lambda_{\mathrm{fin}}}\right)}}$$

$$\mathrm{A_{cb}} = \mathrm{A} + \mathrm{A_{fin}} = \mathrm{wL} + \sum 2(\mathrm{e} + \mathrm{l_{fin}})\mathrm{L}$$

3.3. The heat exchanger

It is described by

$$\mathrm{m_f C_f}\frac{\partial \mathrm{T_f}}{\partial \mathrm{t}} + \frac{\mathrm{mpC_f}}{\mathrm{w}}\frac{\mathrm{dT_f}}{\mathrm{dx}} = \mathrm{h_{cpf}}(\mathrm{T_b} - \mathrm{T_f}) + \frac{\mathrm{A_{cb}}}{\mathrm{A}}\mathrm{h_{cpf}}\mathrm{Eff_p}(\mathrm{T_p} - \mathrm{T_f}) \tag{3}$$

Where mp is mass flow rate ($kg.s^{-1}$), C_f is specific heat ($J.kg^{-1}.k^{-1}$) and w is system width (m) [11-17].

The insulating plate is described by

$$\mathrm{m_b\, C_b}\frac{\partial \mathrm{T_b}}{\partial \mathrm{t}} + \mathrm{U_b}(\mathrm{T_b} - \mathrm{T_a}) = \mathrm{h_{cpf}}(\mathrm{T_f} - \mathrm{T_b}) + \frac{\mathrm{A_{cb}}}{\mathrm{A}}\mathrm{h_{rpb}}(\mathrm{T_p} - \mathrm{T_b}) \tag{4}$$

The back loss coefficient U_b is 0.0692 $W.m^{-2}.k^{-1}$ [11].

4. ELECTRICAL MODEL

The semiconductors p-n junction is a current source which produces the electrical energy (photocurrent) by converting the light flux. Losses arising from junction leakage, contacts and connections resistance are taken into account by shunt (R_{sh}) and series (R_s) resistances. The electrical circuit, modeling a solar cell or a photovoltaic module is represented in the figure 3. The manufacturers give either the I versus V or E_{pv} versus V, curves at different temperatures and power of light, or typical values (I,V) corresponding to short circuit (I_{cc} ,0), or open circuit (0, V_{oc}) current voltage respectively, and maximal power point (I,V). These three pairs of values were measured under standard test conditions of illumination G_{ref} = 1000 $W.m^{-2}$, temperature T_{ref} = 273 K.

$$\mathrm{I} = \mathrm{I_{02}}\left(\exp\left(\frac{\mathrm{q(V-R_sI)}}{\mathrm{N_c\gamma_2 KT_c}}\right) - 1\right) + \mathrm{I_{01}}\left(\exp\left(\frac{\mathrm{q(V-R_sI)}}{\mathrm{N_c\gamma_1 KT_c}}\right) - 1\right) + \cdots \mathrm{I_{0n}}\left(\exp\left(\frac{\mathrm{q(V-R_sI)}}{\mathrm{N_c\gamma_1 KT_c}}\right) - 1\right) + \frac{\mathrm{(V-R_sI)}}{\mathrm{R_{sh}}} - \mathrm{I_l} \tag{5}$$

$$\mathrm{I_l} = \mathrm{I_{ccref}}\frac{\mathrm{G}}{\mathrm{G_{ref}}} + \mathrm{c_{cc}}(\mathrm{T_c}\text{-}\mathrm{T_{ref}}) \tag{6}$$

$$\mathrm{I_0} = \mathrm{I_{0ref}}\frac{\mathrm{T_c}}{\mathrm{T_{ref}}}\exp\left(\frac{\mathrm{qE_g}}{\mathrm{n_s\gamma K}}\left(\frac{1}{\mathrm{T_{ref}}}\right)\text{-}\frac{1}{\mathrm{T_c}}\right) \tag{7}$$

Where I_l, I_{ccref} and I_0 are the photocurrent, reference current of short-circuit and the saturation diode current (in A) respectively, Tc is the temperature of the cells (K) and q is the charge of the electron, K is the Boltzmann constant, E_g is the gap energy (ev), γ is the ideality factor of the junction with values between (1-2) and I_{0ref} is a coefficient dependent on temperature and on the cell technology [18]. G is the illumination ($W.m^{-2}$), I_{cc} is the short-circuit current (A) and c_{cc} is the temperature coefficient of the short-circuit current ($A.K^{-1}$) given by the manufacturer. Following equation (5), it is easy to assume that the current intensity is mainly proportional to the lighting, whereas the other parameters (E_g, I_{cc}, R_{sh}, R_s and γ) vary strongly with the temperature and the technology used [19].

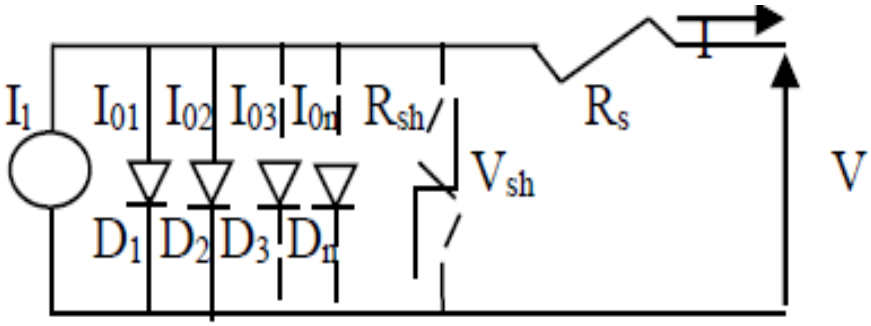

Figure 3. Electrical model

5. HEAT TRANSFER COEFFICIENTS

In the above equations, radiative and convective heat transfer coefficients are calculated using the relations reported in references [15-16].

The radiative heat transfer coefficients from glass cover to sky and absorber plate are taken as [16]

$$h_{rgs} = \frac{\varepsilon_g \sigma (T_g^4 - T_s^4)}{(T_g - T_a)} \tag{8}$$

Where the equivalent sky temperature is evaluated as

$$T_s = 0.0552 T_a^{1.5} \tag{9}$$

$$h_{rpg} = \frac{\sigma((T_p^2 + T_g^2)(T_p + T_g)}{(\frac{1}{\varepsilon_p} + \frac{1}{\varepsilon_g} - 1)} \tag{10}$$

$$h_{rbp} = \frac{\sigma((T_p^2 + T_b^2)(T_p + T_b)}{(\frac{1}{\varepsilon_p} + \frac{1}{\varepsilon_b} - 1)} \tag{11}$$

The convective heat transfer coefficient of the wind is calculated by [11].

$$h_{cgw} = 2.8 + 3V_v \tag{12}$$

V_v: The wind velocity is 3 m/s.

The natural convection heat transfer coefficient between the solar cells and glass cover is calculated as [17].

$$h_{cpg} = \left(\frac{\lambda_a}{H_{pg}}\right)\left(1 + 1.44\left(1\text{-}\frac{1708}{R_a\cos\beta}\right)\left(1 \text{ -}\frac{\sin(1.8\beta)^{1.6}1708}{R_a\cos\beta}\right) + (R_a\cos\beta/5830)^{\frac{1}{3}}\text{-}1\right) \tag{13}$$

The forced convective heat transfer coefficient of cooling air is calculated by [7-10].

$$h_{cpf} = \left(\frac{\lambda_f}{l}\right)(0.0158R_e^{0.8} + (0.00181R_e + 2.92)\exp^{-\frac{0.03795X}{l}} \tag{14}$$

Where, R_e and R_a is Reynolds and Rayleigh numbers [11].

6. METHOD OF CALCULATION

We can write the equation 7 as:

$$\frac{dT_f(x)}{dx} + pT_f(x) = q \tag{15}$$

Where p and q are constants obtained by algebraic manipulations. The boundary conditions are:

$$T_f(x) = T_a, \text{at } x = 0$$

$$T_f(x) = T_0, \text{at } x = L$$

The solution can be obtained as:

$$T_f(x) = \frac{q}{p} + \left(T_a\text{-}\frac{q}{p}\right)\exp^{-px} \tag{16}$$

By grouping the equations from equation 1 to 4, we obtain a four variables matrix. In the equation 16, p and q are the two unknown temperatures. An iterative algorithm is applied to determine these temperatures. In order to calculate the temperature of each cell of the photovoltaic concentrator, the panels is divided into n=252 units of 0.031746 m length (n is also the number of series cells in the collector). To start the calculation, initial values at

T_g, ($T_p = T_{pv}$) and T_b are introduced. The temperature T_f of the air flow at x=0, is equal to the ambient temperature. The new temperatures can be obtained from the matrix. Gauss-Seidel method is used to calculate the temperatures of each cell by an iterative process which is repeated until temperature values converge. Thus, the components temperatures for the first cell can be determined. Applying it as the inlet to the next cell, the components temperatures for the second cell can be similarly calculated. By repeating this step, all temperatures for the different components can be determined. Using these temperatures, one can deduce the air mass flow influence on the cells and panel efficiency

7. PERFORMANCE PARAMETERS

Performance parameters of the hybrid sensor thermal/photovoltaic are computed as following:

The thermal efficiency of the system is:

$$\mathrm{Eff_{th}} = \frac{\sum_{j=1}^{n} m_p C_f (T_{o,j} - T_{i,j})}{AGCo} \tag{17}$$

The electrical efficiency of the system is [10]:

$$\mathrm{Eff_{pv}} = \frac{\sum_{=1}^{n} \tau_g \alpha_{pv} GP \rho_R^n d\left(1 + \frac{\rho_{pv}\rho_g \rho_R^{2n}}{Co}\right)(\mathrm{Eff_{pv,j}})}{GCo} \tag{18}$$

The combined thermal-photovoltaic efficiency is the sum of photovoltaic and thermal efficiencies of the system.

$$\mathrm{Eff_{pvt}} = \mathrm{Eff_{pv}} + \mathrm{Eff_t} - \mathrm{Eff_c} \tag{19}$$

$\mathrm{Eff_c}$: Compressor Efficiency

8. RESULTS AND DISCUSSION

Some main thermo-physical parameters used in the calculation are presented in the Table 1. The dimension of the system is (w*L=2*7.8 m). The dimensions of the fins are ($e*l_{fin}*L$=0.00075*0.025*7.8m). Cells dimensions (w_c*L_c=0.189*0.031746 m). In practice, time variation of the enthalpy of the captor's components, namely the ($mC\frac{\partial T}{\partial t}$) terms are negligible [13]. We can therefore reasonably make the hypothesis of a quasi-stationary operation of the sensor. This hypothesis has the consequence of simplifying the equations without however masking the temporary evolution of the phenomena which remain to the solar flux G variable in the time.

Table 1: Thermo-physical and internal parameters of the system and photovoltaic panels

Parameter	Value	Parameter	Value
α_g	0.04	ε_g	0.86
α_p	0.95	ε_p	0.95
τg	0.9	ε_b	0.95
ρ_g	0.06	q	5.66.10-8 $W.m^{-2}.k^{-4}$
ρ_p	0.06	λ_{fin}	203.6$W.m^{-1}.K^{-1}$
ρR	0.94	C_f	1008 $J.kg^{-1}.K^{-1}$
n	0.61	ρ_{pv}	0.05
Co	2	F	0.52
U_p	0.0692 $W.m^{-2}.k^{-1}$	d	0.95
G_{ref}	1000 $W.m^{-2}$	T_{ref}	273 K
K	1.381.1033 $J.k^{-1}$	R_{sh}	300 Ω
E_g	1.12 ev	R_s	0.75 Ω
q	1.602.10^{-19} c	I_{ccref}	3.8 A
N_s	72	V_v	3 $m.s^{-1}$
$\lambda_a = \lambda_f$	0.044 $W.m^{-1}.K^{-1}$	e	0.00075 m
l_{fin}	0.025 m		

The time dependent values of solar irradiation G and ambient temperature Ta, used for the calculation are shown on figure 4.

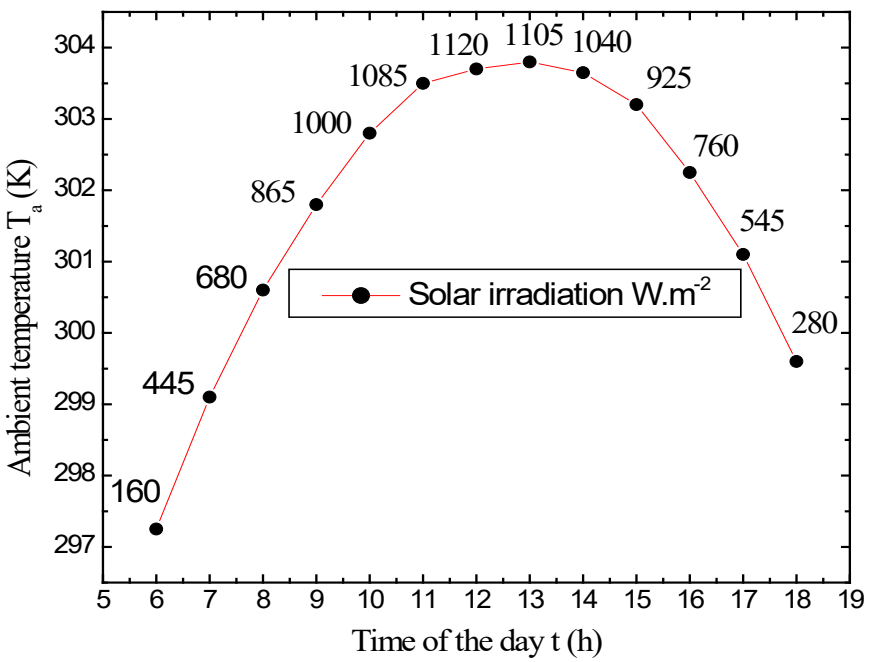

Figure 4: Mean hourly values of the solar radiation G and the ambient temperature in Constantine.

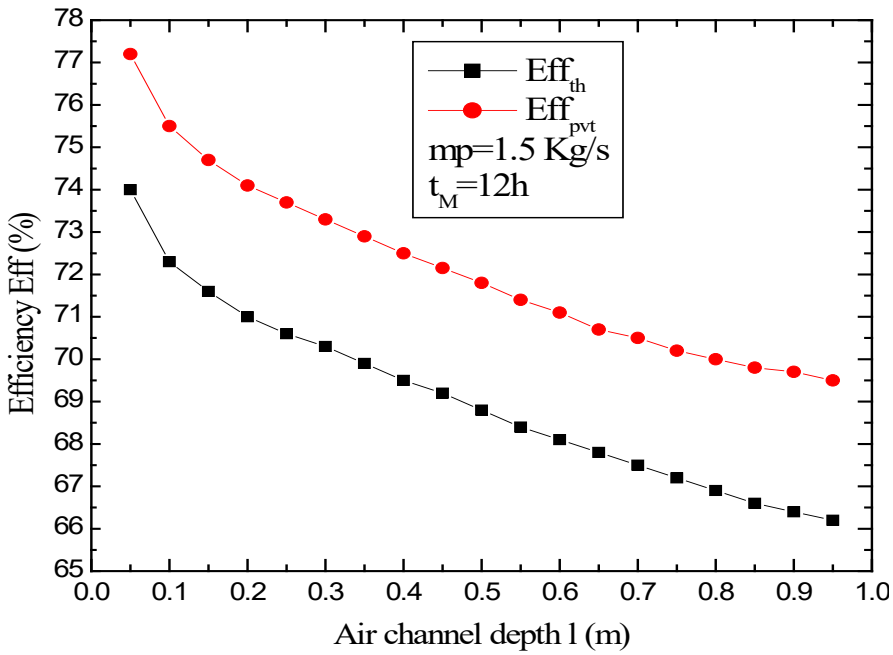

Figure 5: Effect of the thermal efficiency, and photovoltaic-thermal efficiency on the air channel depth

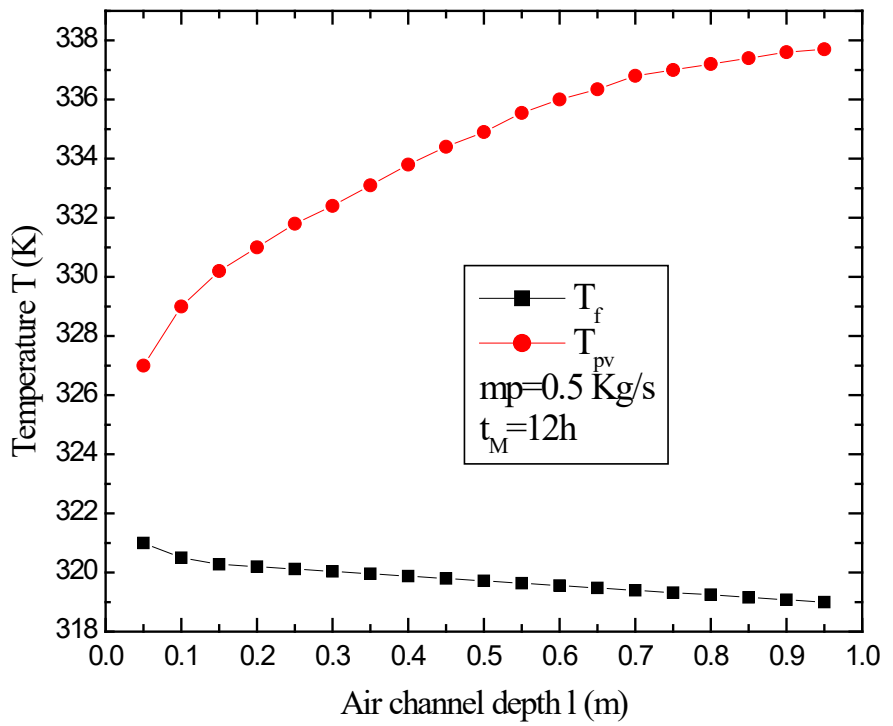

Figure 6. Effect of the photovoltaic and fluid temperatures on the air channel depth

The Figure 5 shows the effect of air channel depth of heat exchanger on the thermal, photovoltaic-thermal efficiency and mass flow rate for 12h of sunshine. The figure 6 shows the effect of air channel depth of heat exchanger on the outlet fluid and photovoltaic temperatures. Photovoltaic temperature constant increases when one increases the air channel depth of the heat exchanger. This is explained by the fact that the heat exchanges internal convective in the sensor between air and the cells improved, when the distance between absorber and insulating plate, decreases. The outlet air temperature and the efficiency of the system decrease with increasing air channel depth (Figure 5 and 6) because the internal thermal convective exchanges deteriorate with increasing air channel depth, the air flow rate being kept constant. We observe that the photovoltaic temperature increases quickly with increasing the air channel depth of the exchanger of heat, and maintaining the mass flow of air constant(Figure 6).To keep the photovoltaic temperature constant and minimize the mass flow as much as possible, it is necessary to decrease the air channel depth this is explained in (Figure 7), in (Figure.8) It is observed that the efficiency photovoltaic-thermal (daily output) of the system decreases when one increases the air channel depth of the heat exchanger. This is explained by the fact that the heat exchanges connectives internal in the sensor deteriorate, when the distance between absorber and insulating plate, increases, the mass flow of air being maintained constant.

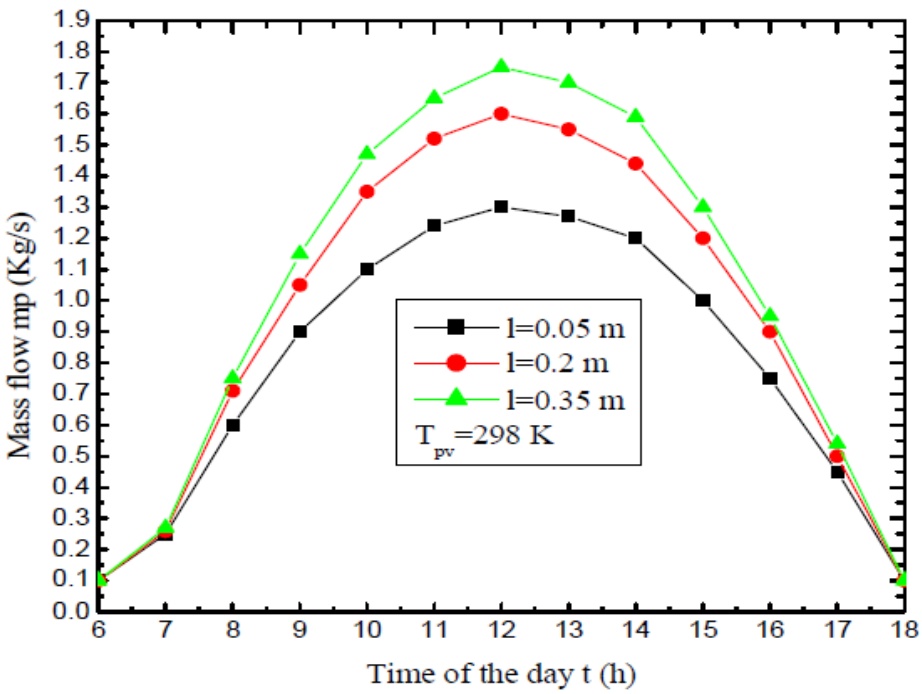

Figure 7. Effect of the air channel depth on the hourly variations of the mass flow

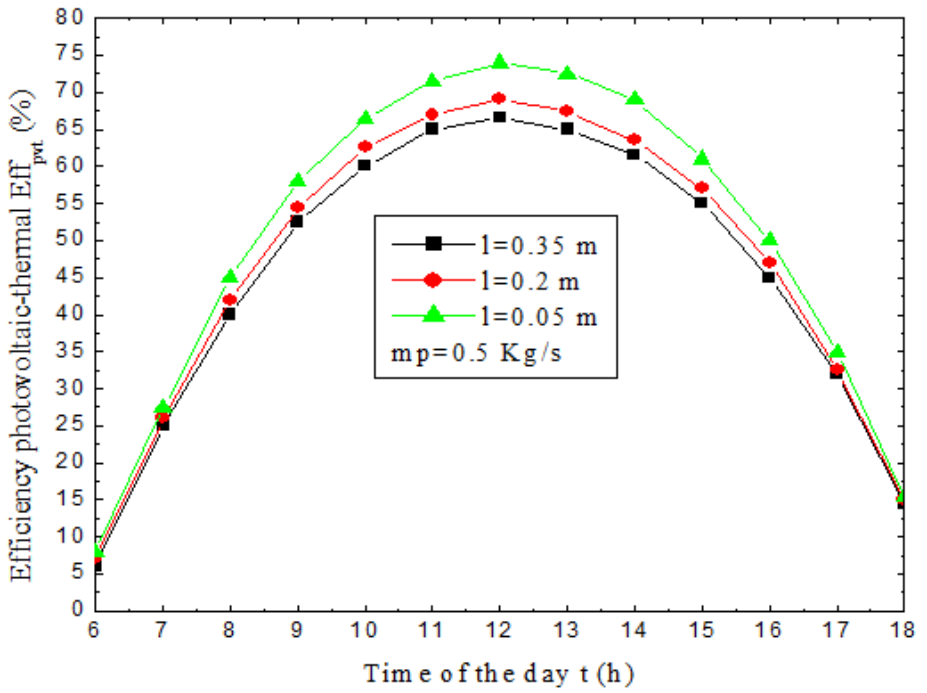

Figure 8. Effect of the air channel depth on the hourly variations of the efficiency

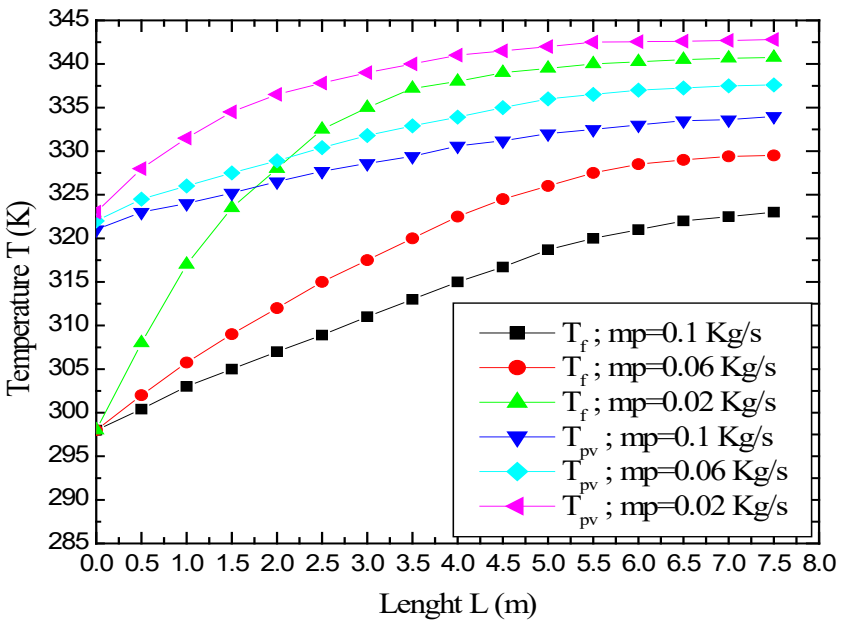

Figure 9. The mass flow rate influence on the fluid, cells and insulating plate temperature

The Figure 9 shows the effects of the mass flow rate on the fluid, and photovoltaic temperature respectively as a function of the position along the panel length. It can be observed that all the temperatures, increase with the position. Increasing of the air mass flow rate will decrease the temperature of the system, at constant sunlight radiance. This is explained by the increase of air amount at a given heat load, leading to a reduction of its temperature exit. The figures 10 and 11 show the effect of the mass flow on thermal and electrical efficiency of the system respectively in the air flow direction. The thermal and electrical efficiency increases in the air flow direction. The electrical efficiency increasing is linear and we have a small increasing in the curves when the mass flow increases in the range higher than 3m along the air flow direction. The thermal efficiency increases in as exponential form in the air flow direction and is very important when the mass flow increases (figure 10). This is due to the improvement in internal convective exchangers at a constant heat loss when the air flow increases. The thermal efficiency of the system is increasing from 18% to 55%, when a mass flow rate varies from 0.02 kg/s to 0.1 kg/s.

The Figures 12, 13 and 14 shows the mass flow rate influence on the photovoltaic-thermal efficiency, the electric power of each cell and electric power of the sensor respectively in the air flow direction. The curve of the electric power of sensor is identical in a length smaller than 3m but above 3m there is small increase when the mass flow is increasing, and the difference in the photovoltaic-thermal efficiency is important with the increasing of the mass flow. This trend is explained by the fact that when the mass flow increases, the cells are cooled which increases the electric power and the photovoltaic-thermal efficiency. Note that the

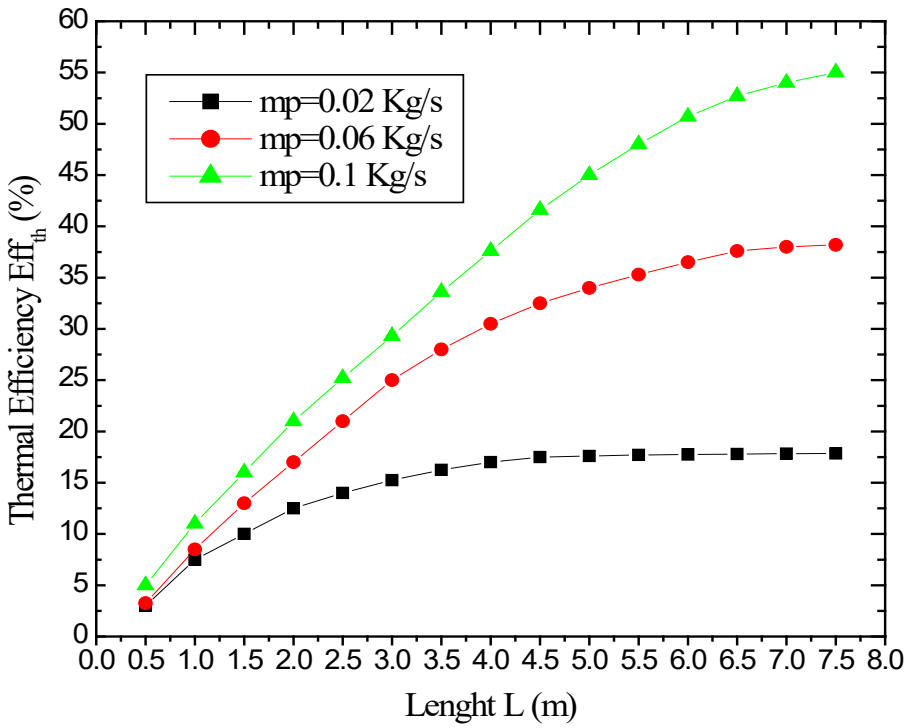

Figure 10. The mass flow rate influence on the thermal efficiency

power of each cell decreases in the air flow direction when the temperature increases. For a given point in the sensor length this value increases because the mass flow rate increases. The photovoltaic-thermal efficiency of the system is increasing from 25% to 60%, when the mass flow rates vary from 0.02 kg/s to 0.1 kg/s (Figure 12).

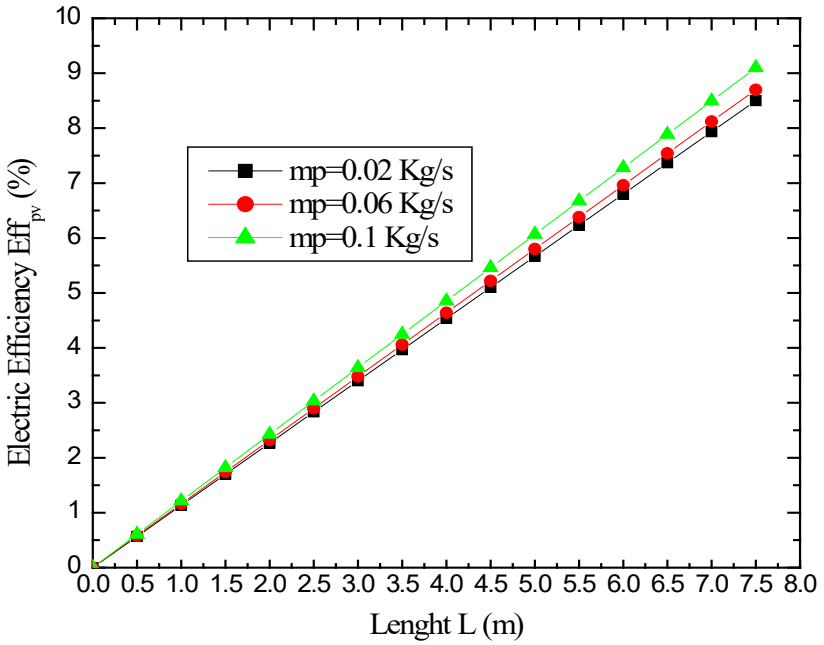

Figure 11. The mass flow rate influence on the electric efficiency

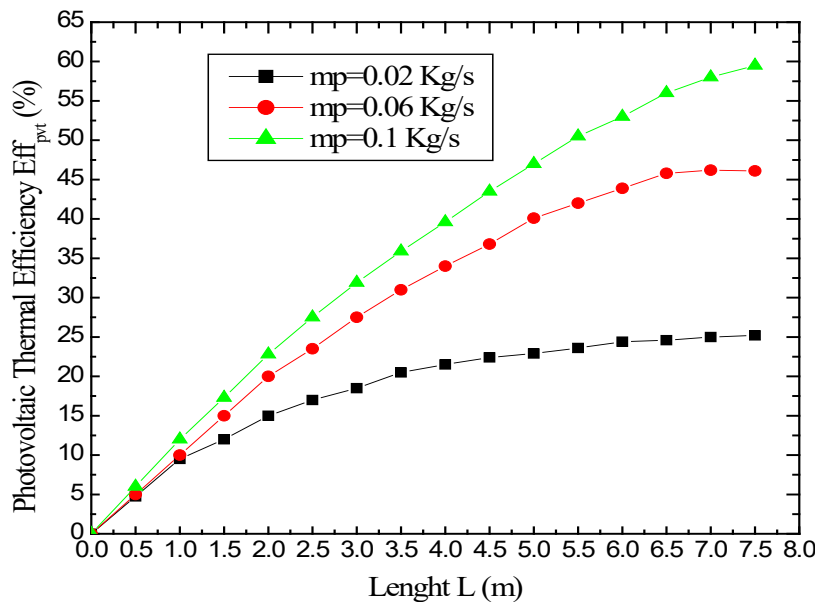

Figure 12. The mass flow rate influence on the photovoltaic-thermal efficiency

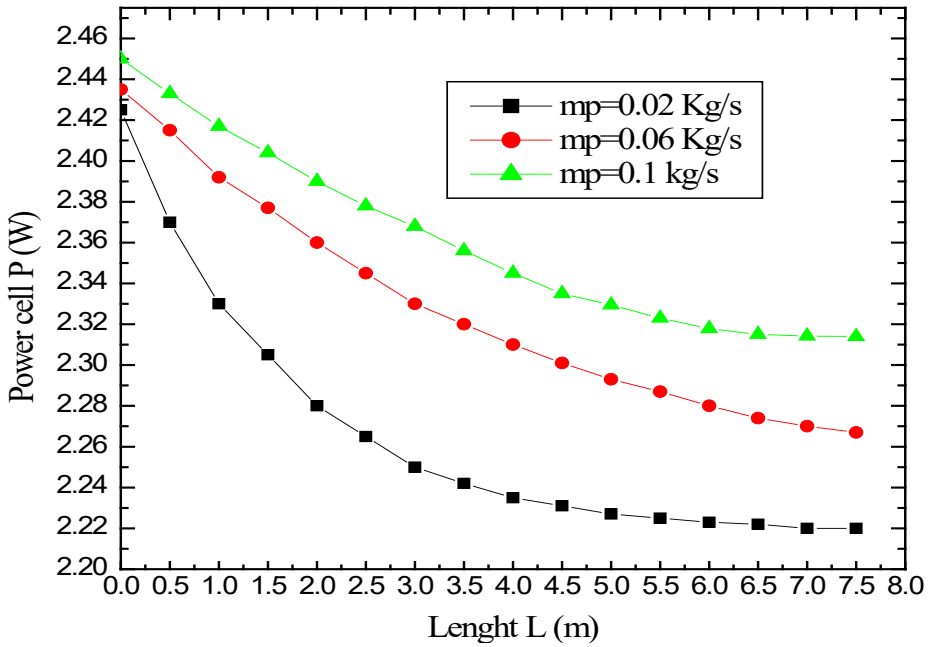

Figure 13. The mass flow rate influence on the electric power of each Cell

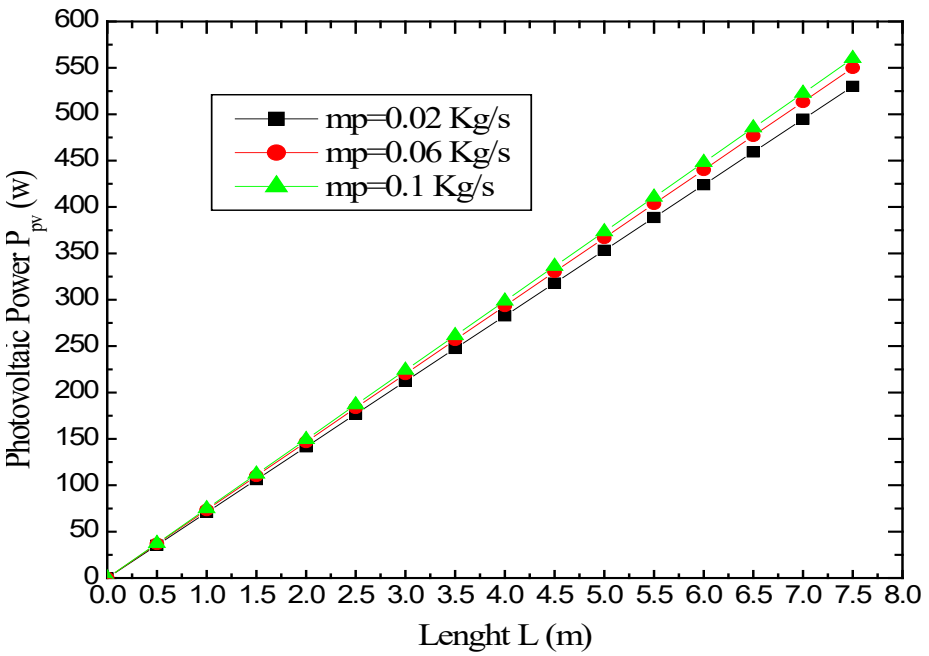

Figure 14. The mass flow rate influence on the electric power of sensor

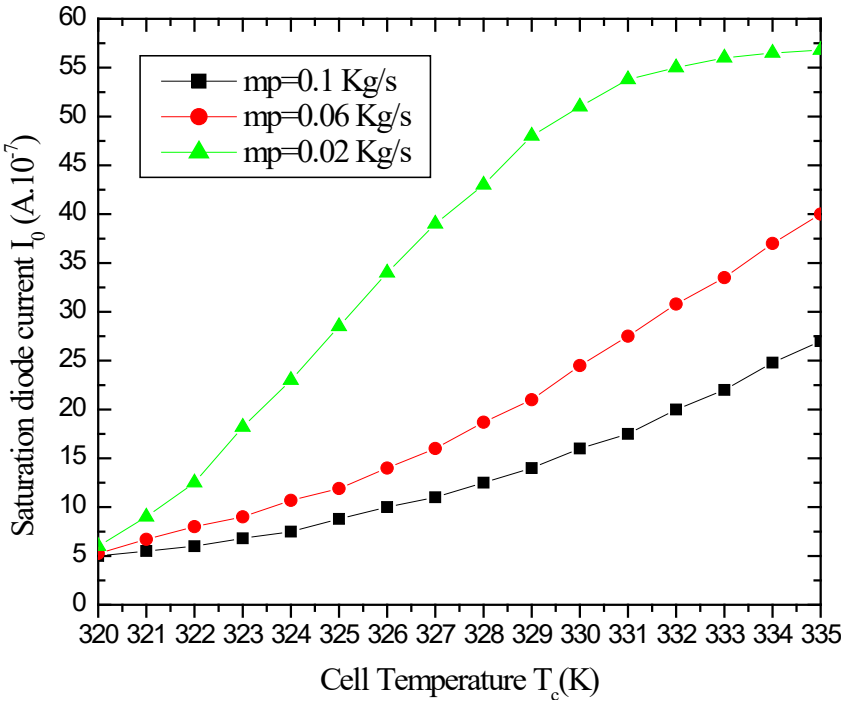

Figure 15. The variation of the reference current according in the cell temperature reel

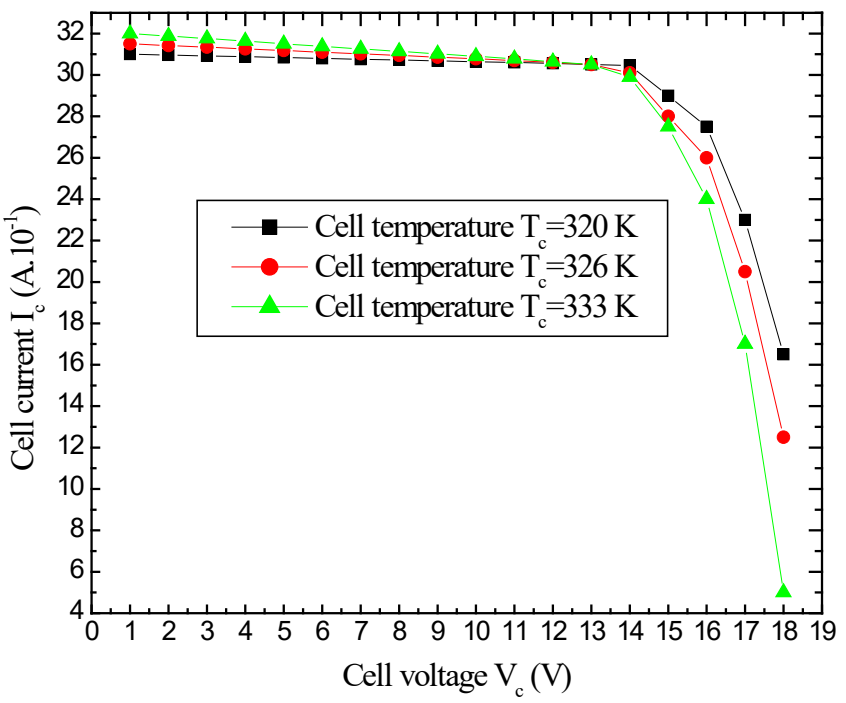

Figure 16. The variation of the panel current according on the panel voltage

The variation of the saturation current as a function of the cell temperature is shown in the figure 15. When the cell temperature and the losses by the joule effect increase, the saturation current increases, therefore the each cell electric power decreases. In the same figure if the mass flow increases, the reference current at a given position, decreases. This is induced by the four that the increase of the mass flow rate strongly cools the cells. If we consider the figure 16, we deserve that the current decreases when the temperature increases. This is consistent with the physical principles governing cells behavior. Indeed, the current (I) is proportional to the mobility and the density of electrons and holes. When the carrier's density is constant in the used temperature domain, the current at constant, voltage is proportional to the carrier's mobility. It is known that the carrier's mobility decreases when the temperature increases. This is due to the strong diffusion of the charge carriers by, the crystalline lattice and localized doping atoms photons. This diffusion decreases the carrier's mobility, and the electric current, which is in agreement with our results.

9. CONCLUSION

In this study, heat transfer and the semiconductors p–n junction equations are used to study effect of the air channel depth of heat exchanger and the air mass flow rate on efficiency of solar concentrating photovoltaic thermal air system. A theoretical model for the energy analysis is presented. From this simulation it can be stated that, the efficiency and the fluid temperature of the concentrating photovoltaic thermal air system, increases with decreasing of channel depth of heat exchanger. In resume time the temperature decreases. We have shown that the amount of heated air rises with the air mass flow rate increasing. This causes a decrease in the outlet temperature which then cools, the solar panel, owing to an improvement in the internal convective heat transfer. Consequently, the thermal and the electrical performance of the system are enhanced. The increase of the electrical efficiency for solar cells following the decrease in their temperature has a beneficial effect on the electrons and holes mobility. This carrier mobility increases as the temperature decreases. Based on this analysis, the appropriate operating conditions for concentrating photovoltaic thermal air system could be determined with the given conditions and are useful for obtaining a higher useful energy rate and decreasing internal losses. We conclude that once the developed simulation model is successfully verified by experimental results, this model will useful at different operating conditions such as exchanger channel width, flow rates, inlet temperatures, sizing and so on.

REFERENCES

[1] Kern Jr E C, Russell M C, Combined photovoltaic and thermal hybrid collector system, In: Proceedings of 13th IEEE Photovoltaic Specialist. (1978),1153—1157.

[2] L.W. Florschuetz, Extension of the Hottel-Whillier model to the analysis of combined photovoltaic thermal flat collector, Sol Energy Vol. 22 (1979),361-366.

[3] H.P. Garg, R.S Adhikari, Conventional hybrid photovoltaic thermal (PV/T) air heating collectors: Steady-state simulation, Renewable Energy Vol.11 (1997), 363-385.

[4] H.P. Garg and R.S. Adhikari, Performance analysis of a hybrid photovoltaic/thermal (PV/T) collector with integrated CPC troughs, Int. J. Energy. Res Vol. 23 (1999), 1295-1304.

[5] G. Palani and E. J. Lalith Kumar, heat and mass transfer effects on a free convective flow past a semi-infinite vertical cone with thermal radiation and chemical reaction, JP Journal of heat and mass transfer Vol.9 (2011), 103-129.

[6] G.R. Whitfield, R.W. Bentley, C.K. Weatherby, B. Clive, The development of small concentrating pv systems, Proc. of 29th IEEE PVSC. New Orleans. (2002), 1377-1379.

[7] M.Y. Othman, B. Yatim, Performance analysis of a double-pass photovoltaic/thermal (PV/T) solar collector with CPC and fins, Renewable Energy Vol. 30 (2005), 2005-2017.

[8] X. Chen, Y.M. Xuan, Y.G. Han, Investigation on performance of a solar thermophotovoltaic system, Sci. China. Ser. E-Tech. SciVol.51(2008), 2285-2294.

[9] S. A. Nada, W. G. El Shaer and A. S. Huzayyin heat transfer and pressure drop characteristics of multi tubes in tube helically coiled heat exchanger, JP Journal of heat and mass transfer Vol.9 (2011),173 – 202.

[10] Koutama Amara, RidhaChouikh and AmenAllahGuizani, heat and mass transfer analysis in a rotary wheel, JP Journal of heat and mass transfer Vol.9 (2011),1-12.

[11] R. Ari, Optical and thermal properties of compound parabolic concentrators, Sol. Energy Vol.18 (1976), 497-511.

[12] K. Sopiana, H.T. Liu, S. Kakac, T.N. Veziroglu, Performance of a double pass photovoltaic thermal solar collector suitable for solar drying systems, Ener. Conv. Manage Vol. 41(2000), 353-365.

[13] S. Sharples, P.S. Charlesworth, Full-scale measurements of wind- induced convective heat transfer from a roof-mounted flat-plate solar collector, Sol. Energy Vol.62 (1998), 69-77.

[14] S. Srinivas, T. Malathy and A. Subramanyam Reddy, analysis of heat and mass transfer on pulsatile flow in an inclined porous channel with thermal-diffusion and chemical reaction, JP Journal of heat and mass transfer Vol.9 (2011),57-100.

[15] S.J. Anand, T. Arvind, Energy and exergy efficiencies of a hybrid photovoltaic–thermal (PV/T) air collecto, Renewable Energy Vol.32 (2007), 2223-2241.

[16] A. Duffine, W.A. Beckman, Solar Engineering of Thermal Processes, John Wiley & Sons, New York, (1991).

[17] G. Walker, Evaluating MPPT converter topologies using a MATLAB PV model, J. Electr. Electron. Eng Vol.21 (2001), 49–56.

[18] R. Kadri, H. Andrei, J. P. Gaubert, T. Ivanovici, G. Champenois, P. Andrei, Modeling of the Photovoltaic Cell Circuit Parameters for Optimum Connection Model and Real-Time Emulator with Partial Shadow Conditions, Energy Vol.42, (2012).

[19] Ramos Hernanz, JA., Campayo Martín, J.J., Zamora Belver, I., LarrañagaLesaka, J.,Zulueta Guerrero, E., Puelles Pérez, E, Modelling of Photovoltaic Module, Conference on Renewable Energies and Power Quality (ICREPQ'10) Granada (Spain), March,(2010).

NOMENCLATURE

A	Area	m^2
C	Specific heat	$J.Kg^{-1}.K^{-1}$
c_{cc}	Temperature coefficient of the short-circuit	$A.K^{-1}$
Co	Ration concentrating	
d	Correction of gap loss	
E	Energy	J
e	Thickness fin	m
Eff	Efficiency	
Eg	The gap energy	ev
F	Solar cell packing factor	
G	Solar irradiation	$W.m^{-2}$
h	Heat transfer coefficient	$W.m^{-2}.K^{-1}$
H_{pg}	Height (plate-back loss)	m
I	Current	A
L	Length	m
l	Air cannel depth	m
m	Mass flow rate	$Kg.m^{-2}$
mp	Mass flux	$Kg.s^{-1}$
q	Charge of the electron	c
R_a	Rayleigh number	
R_e	Reynolds number	
R_s	Resistance serie	Ω
R_{sh}	Resistance shunt	Ω
T	Temperature	K
t	Time	s, h
U	Back loss coefficient	$W.m^{-2}.K^{-1}$
V	Voltage	V
V_v	Velocity	$m.s^{-1}$
w	System width	m
x	Direction variable	m

Greek letters

α	Absorptivity	
τ	Transmitivity	
ρ	Reflectivity	
Υ	Ideality factor	
ρ_R	Reflector	
λ	Thermal conductivity	$W.m^{-1}.K^{-1}$
σ	Boltzmann number	$W.m^{-2}.K^{-4}$
ε	Emissivity	
β	Acceptance angle	$(^0)$

Subscripts

a	Ambient
b	Back plate
c	Cell
cb	Bottom surface of absorber plate
cc	Short circuit
cgw	Convection (glass-wind)
cpf	Convection (plate-fluid)
cpg	Convection (plate-glass)
ct	Top surface of absorber plate
f	Fluid
fin	Fin
g	Glass
l	Photo
o	saturation
ov	Open circuit
p	Absorber plate
pv	Solar Cell (photovoltaic)
pvt	Photovoltaic- Thermal
ref	Reference

rgs Radiation (glass-sky)

rpb Radiation (plate-back plate)

rpg Radiation (plate-glass)

s Sky

th Thermal